JTTEE 3:148-161

Controlled Microstructure of Arc-Sprayed Metal Shells

P.S. Fussell, H.O.K. Kirchner, F.B. Prinz, and L.E. Weiss

Shells made of sprayed ferrous materials are feasible for prototype and limited production tooling. A systematic study of the microstructure of arc-sprayed ferrous structures is presented, demonstrating why these structures display a degree of mechanical anisotropic behavior. The results of controlling oxide formation with inert atomization gases are given, and methods for tailoring the composition and orientation of the lamellae through robotically controlled deposition are discussed.

1. Rapid Tooling

RAPID manufacturing of tooling for injection molding, stamping, composite lay-up, or similar processes where the shape of the tool is critical is a challenging problem with considerable commercial potential (Ref 1). The creation of such tooling by the arc spraying of zinc and zinc alloys has been reported in the commercial literature for at least 25 years (Ref 2), and thick-sprayed zinc structures have been documented for 65 years (Ref 3). These alloy systems, however, are relatively soft and prone to wear and loading failure; therefore, their usefulness is largely limited to prototype tooling applications and low pressure applications, such as reaction injection molding tooling. Tools made from ferrous systems (Ref 4, 5), as shown in Fig. 1, are of far greater applicability, both for superior prototyping and limited production. They have much greater wear resistance than zinc systems, are stronger, and withstand the demands of elevated-temperature service. Furthermore, the demands of the injection molding application are well matched to the ferrous shell structures produced by arc spraying, particularly the support of hoop stresses in the tool structure, the tolerance of compression in the ferrous shell, and the tool face wear resistance to abrasive plastics such as glass-filled nylon.

The authors' system uses a computer-based geometric modeling program called NOODLES (Ref 6) to describe the part and patterns needed to make the mold or die. A solid free-form fabrication process—in this case, a stereolithography apparatus—autonomously creates the pattern in a matter of 1 or 2 days; complex patterns can require up to 30 days if fabricated by conventional processes. The shells are fabricated by robotically spraying metal using an arc-spray device to create the tooling face and structure. The backside of the tooling cavity is then filled with a support material to sustain the compressive service loads. Figure 2 shows a cross section of such a tool. The material-choice aspects of this problem are made complex by the elevated service temperatures (as high as 450 °C); it is desirable to match the coefficients of thermal expansion of the sprayed tooling material and the backing material.

The synergy of a coherent, computer-based, three-dimensional modeling system, a rapid prototyping fabrication device, and a robotically based spraying system has made this approach for manufacturing low-volume tooling economically appealing, particularly for geometrically complex shapes. The time needed to manufacture such a tool is about 1 week; the cost of the manufactured tool is substantially less than a conventionally made one-of-a-kind mold or die.

The direct linkage of the part's computer model and the part's tooling results in paperless manufacture; changes in the geometry of the part are directly communicated to the next iteration of tooling, and unacceptable aspects of the design, from a manufacturing perspective, are communicated back to the computer model. Using the robot to manipulate the arc-spray gun has three

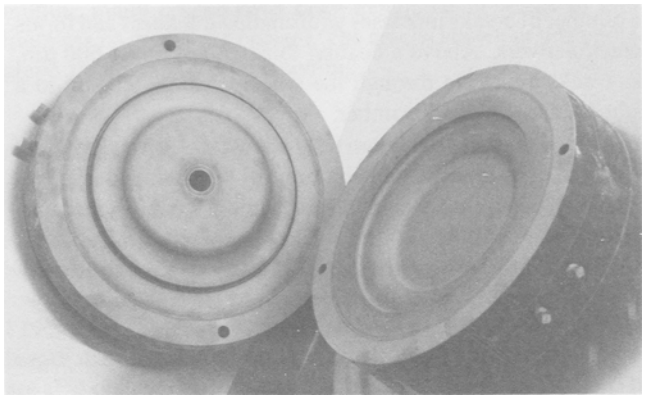

Fig. 1 Type 420 stainless steel sprayed injection mold for a flying disk

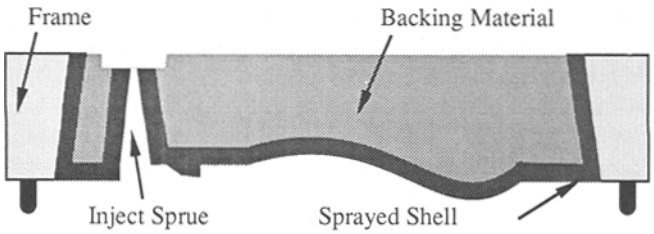

Fig. 2 Schematic cross section of a sprayed tool. The frame interior is angled to help support compressive loads on the tool face

Key Words: arc spray process, manufacturing, microstructural effects, near net shaping, rapid tooling, robotics, sprayed tooling

P.S. Fussell, Alcoa Laboratories, Alcoa Center, PA 15069; **H.O.K. Kirchner**, Institut de Sciences des Matériaux, Université Paris, Orsay, Cedex, France; **F.B. Prinz**, Engineering Design Research Center, Carnegie Mellon University, Pittsburgh, PA 15213, USA; and **L.E. Weiss**, Robotics Institute, Carnegie Mellon University, Pittsburgh, PA 15213, USA

striking advantages: Any particular schedule for spraying a mold or die half is repeatable; moreover, the robot is precise—meaning, for example, that an intended standoff of 10 cm is precisely executed; and the robot is reprogrammable for new tooling designs. This combination yields immediate benefits in the quality of sprayed ferrous alloy shells. The robotic repeatability is required for consistency in the sprayed shell, as well as consistency in this experimental work. The robot, being a programmable mechanism with considerable freedom of motion, is also capable of spraying complex surface geometries.

The basic fabrication of these sprayed ferrous tools had been problematic. In making sprayed tooling, metal is first sprayed onto a substrate and then removed from that substrate; thus, the interface layer between substrate and coating is by design weak in order to permit separation.

After the arc spraying is completed, the shell and the substrate still contain considerable internal stress, albeit in equilibrium. These thermally induced stresses can be very large (Ref 7). When the shell is separated from the substrate, the shell deforms as it comes to a new equilibrium. Current process art limits this to roughly 1 mm deflection in 500 mm length of shell for a 2 mm thick shell. Secondly, the sprayed shells are backed with a mass castable ceramic or filled epoxy, principally to provide tool compressive strength. If the shell and the backing material have different coefficients of thermal expansion, then the normal thermal cycling of a tool will create shear at the shell/backing interface. The presence of internal stress in the shell, as well as a mismatch of coefficients of thermal expansion, also raises questions of the geometric stability of the shell at elevated temperatures and over long periods of time. Finally, the spray process is poorly suited for spraying into narrow channels and small-aspect-ratio holes.

As much of the function of a tool is determined by its geometry, much of the strength and wear characteristics of a tool are determined by the microstructure of the sprayed shell. The focus of this work is the microstructure of the sprayed shell, with emphasis on designing aspects of the microstructure to meet the demands placed on the inner shell of the tool.

2. Metal-Spraying Techniques

2.1 *Osprey, Plasma, and Flame Techniques*

A variety of techniques are available for depositing metal by a spray process. The Osprey process (Ref 8, 9) provides large deposition rates (1000 kg/h) by atomizing a molten stream of liquid drawn from a pool of liquid metal. This is generally done in a chamber under inert conditions. It is possible to superheat the liquid pool. The deposition rates are such that a contiguous liquid surface is present on the substrate.

At the other end of the spectrum, plasma systems (Ref 10-14) deposit material at a rate of 0.1 to 5 kg/h. These systems function by propelling powdered material in a stream of gas heated by an electrical arc; gas temperatures are reported to be as high as 20,000 K (Ref 14). Deposition rates above several kilograms per hour are difficult to achieve, because typically the powder particles are not entirely melted. Plasma systems permit a wide latitude in choice of materials, as well as good control of the resulting microstructure; therefore, they are mostly used for coating applications.

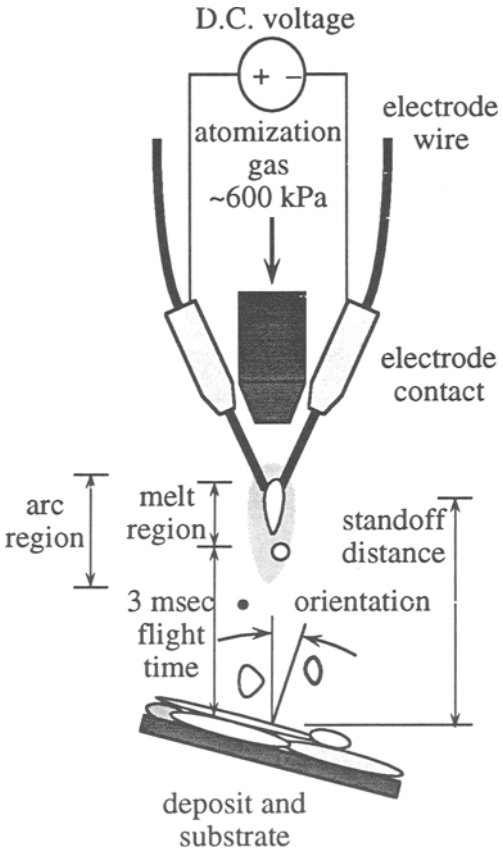

Fig. 3 Schematic of an arc-spray gun and deposited particle flight times

Flame systems maintain deposition rates between 4 and 20 kg/h. As this process essentially uses a heating torch, the substrate is heated, while the particles are conveyed in a gas stream of combustion products. High-velocity variants of flame and plasma systems greatly increase the kinetic energy of the particles and reduce the porosity of the sprayed material. The high-speed flow of molten material can also serve as an abrasive to the substrate.

2.2 *Arc Spraying*

The work reported here uses an arc-spray system (Ref 15, 16). It is comparable in cost to the low-cost flame system (while avoiding the inherent products of combustion), is extremely easy to operate, and uses widely available feedstock materials (any conductive material, such as welding electrode wire, that can be drawn into a wire).

The arc-spray gun is shown in Fig. 3. Two consumable electrode wires are fed through contact tips to the area of the arc. A dc power supply establishes an arc between the wires, melting them in the arc. A column of atomizing gas, ranging from 480 to 690 kPa (70 to 100 psi), ablates the molten material from the wires, atomizes the molten droplets, and carries them, in a spray, to the substrate. For steel systems, the arc voltage typically ranges from 26 to 31 V; the arc current ranges from 50 to 300 A,

Table 1 Qualitative effect of parameters on spray characteristics

Parameter	Porosity	Oxide	Particle	Particle temperature	Heat load on shell	Orientation of laminae
Standoff distance	o	o		•	•	
Orientation	•					•
Travel speed					•	
Gas pressure	•	o	•	o	o	
Energy of arc	o	o	o	•	•	
Material deposition rate	o		o	o	•	

• implies first-order contribution; o implies a lesser influence

giving a temperature of 10^4 K in the arc (Ref 14). Deposition rates for an arc-spray system range from 1 to 20 kg/h.

The structures resulting from the arc-spray process are suitable for the tooling applications at hand (Ref 16, 17), and the arc-spray process permits a deposition rate that allows a timely buildup of the tool shell thickness. At the same time, the pattern substrate and the already deposited material are not subjected to excessive heat load. Finally, the process is not particularly abrasive, so relatively delicate pattern substrates can be used to provide the shape of the tool. In exchange for lower particle speeds, arc-sprayed materials display a higher porosity. This will affect the fatigue life of the tool, as well as the strength of the material.

2.2.1 Arc-Spray Parameters

Within the arc-spray process, a number of parameters can be controlled to affect the quality of the deposited shell (Ref 18, 19) including:

- Standoff distance: the distance the particles must travel from arc to substrate
- Gun orientation: the orientation of the spray gun with respect to the substrate surface normal, and thus the direction of impact of the sprayed particles upon the substrate
- Traverse speed of the spray gun over the substrate: This directly affects the flux of particles arriving at the substrate.
- Gas pressure: the atomization and accelerating gas pressure in the spray gun
- Arc energy: the energy being consumed in the arc. The resistance of the arc is essentially constant at a constant material consumption rate, so the arc power (and hence the arc specific energy) is set by the power supply voltage.
- Material consumption rate: the amount of material being presented to the arc per unit time; specified as a feed rate of the consumable electrode. Not all of this material is deposited; a fair proportion is lost to overspray, perhaps as much as 50% in some circumstances.

Table 1 shows an overview of the relationship between these parameters and some effects in the spray and shell microstructure.

2.2.2 Solidification and Microstructure

The aim is to influence the microstructure of the shell indirectly by directly influencing the characteristics of the spray. The porosity and oxide levels should be kept at a minimum (ideally zero), and the particle sizes should be uniform, each with a uniform temperature, while imparting no heat load onto the substrate or previously sprayed shell. A measure of compromise is needed in setting the spray parameters.

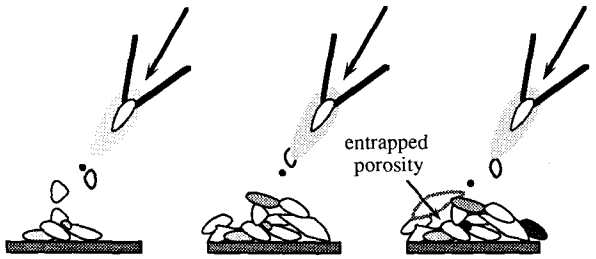

Fig. 4 Schematic of the shadow effect of porosity formation

As shown in Table 1, porosity can be most directly influenced by either increasing the particle kinetic energy or increasing the time for coalescence on the substrate; higher gas pressure, increased particle standoff distance (and therefore speed), and additional superheat to the particles are the means to this end. Orientation has a first-order effect on porosity for shadowing reasons: Previously deposited particles will act as obstructions to incoming particles; worse, the hole formed in the shadow of a previously deposited particle is large and is clustered with other such holes. Figure 4 schematically shows this effect, and the microstructure that is formed will be discussed later in this paper (see Fig. 16). Orientation angles greater than 30° lead to unacceptable porosity. Oxide formation is a kinetic reaction, so, beyond eliminating or reducing oxygen in the vicinity of the molten metal or lowering the temperature of the reacting products, reducing the time for the formation of oxides is of significance; this matches the increase of kinetic energy for porosity reasons. Particle size is principally determined by atomization in the arc; coalescence in the arc and on the substrate is a minor secondary factor in arc spraying. Beyond the first layers deposited, the orientation of the built-up laminar structure is controlled exclusively by the orientation of the torch. Individual lamella morphology is a function of both particle size and orientation of the torch with respect to the substrate surface. The impact of the molten particles on the substrate is greatly influenced by the angle between the particle trajectory and the local surface normal; orientations increasingly distant from the surface normal produce a more fragmented lamella. This effect, combined with the shadow effect, produces undesirable microstructural features.

There is room for considerable improvement in the arc-spray process (Ref 15); for example, nozzle designs should be directed to create a cone of narrow and sharp spatial definition, while maintaining a uniformly hot, homogeneous beam of sprayed material. Synergic power-supply technology routinely available in the arc-welding domain could be applied to better control the formation of metal droplets in the region of the arc.

Unsophisticated methods of depositing metal shells results in poor quality. Spraying with the intention of creating sound microstructures has lead the authors to investigate methods of making shells with lower oxide levels, lower porosity, oriented lamellae, and shells built of sprayed composites.

3. Experimental Arrangement

The experimental arrangement used in this work is organized around a robotically moved arc-spray gun. Both the robot and the arc-spray system are coordinated by an IBM-AT (IBM Corporate Hqtr, Armonk, NY) computer. The design and modeling work is done on 12-MIP class workstation computers of various makes. The arc-spray gun and power supply are commercial products (the gun is a Miller BP-400 (Miller Electric Mfg. Co., Appleton, WI) and the power supply is a Miller Mogularc 400R (Miller Electric Mfg. Co., Appleton, WI)); the arc-spray controller is a Miller custom-built process controller that is interfaced to and controlled by the external computer, which sets the wire-feed rate and arc voltage, as well as starts and stops the arc process. The robot is a GMF S-700 6 (Green Mountain Foam Products, RR, Underhill, VT) axis robot, with additional degrees of freedom in a rotating table. Programs are uploaded and downloaded through the IBM-AT computer, which also initiates robotic motion. The robotic manipulator provides a high degree of motion repeatability in making the sprayed structures; the computer-controlled power supply and arc-spray system lend a similar repeatability to the process variables in the sprayed structures.

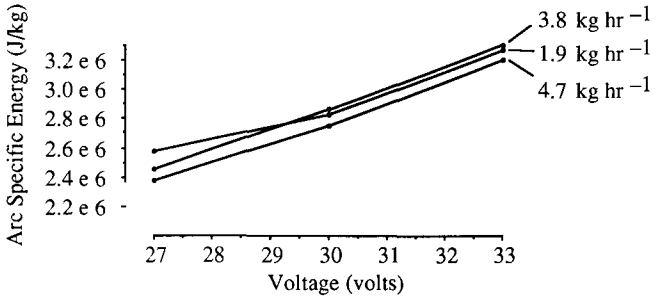

Fig. 5 Arc voltage versus arc specific energy for type 420 stainless steel 1.6 mm diam wire, with the deposition rate as parameter. Essentially, the energy per unit mass melted is proportional to the control voltage, but is independent of the deposition rate.

For a given deposition rate, the arc current and arc resistance are relatively constant as the arc voltage is varied; thus, the power consumed in the arc is largely controlled by the voltage setting. Figure 5 shows the effect of increasing arc voltage on specific energy, with all other variables held constant. With this type of equipment, this is the simplest way to increase the energy available to heat the metal particles.

The experiments were conducted at the lower end of the arc-spray parameter ranges, with a deposition rate of about 2.0 kg/h and a specific energy expenditure of 2.6 MJ/kg (0.74 kW·h/kg) of metal consumed. With the programmed torch travel speed of 500 mm/s, a deposit of 0.1 mm was applied during each cycle of 24 passes. In all cases, the standoff distance was 16.5 cm (6.5 in.) from the arc to the substrate. Similarly, the orientation was, ex-

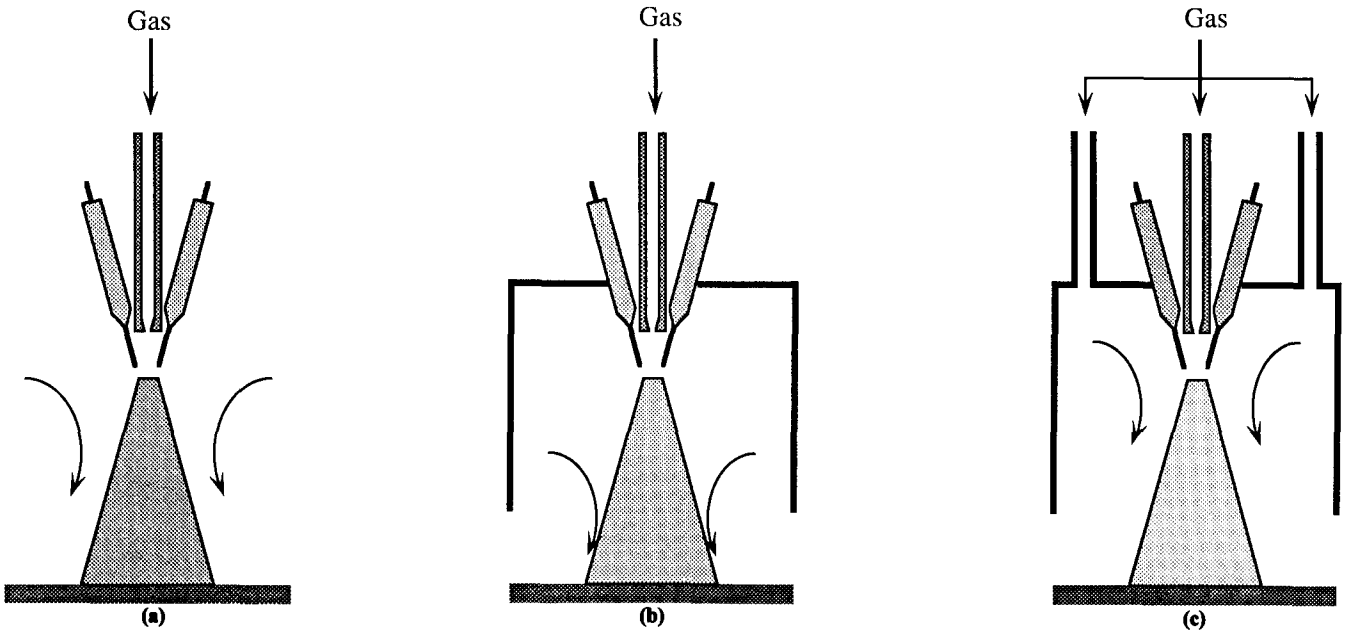

Fig. 6 Shroud arrangement for inert atomization and cover gas. (a) No protective cover. (b) Protective shroud. (c) Protective shroud with protective gas flow

cept as noted below, normal to the substrate (i.e., the particles traveled along a course parallel to the surface normal).

The atomizing gas in the experimental facility comes either from an air compressor (capable of suppiying 1.2 MPa, or 175 psi, pressure) or from a cluster of compressed gas bottles. The process produces a broad spectrum of particle sizes, ranging from +100 μm diam particles to submicron particles.

Because of the large surface/volume ratio of the sprayed droplets, oxidation in flight and after impingement is a problem. The obvious way to circumvent the detrimental effect of oxidation and avoid the ensuing brittleness of the deposit is to minimize the partial pressure of oxygen in the gaseous atmosphere (Ref 20) and to keep turbulence as low as possible. The influence of these factors was studied by choosing three experimental setups, as shown in Fig. 6. Either the robotically manipulated jet was directed toward the substrate without any protective cover (Fig. 6a), or it was protected by a shroud (Fig. 6b) that minimized turbulence of the surrounding atmosphere. In this arrangement the hot jet and deposit are mainly flushed by the gas of the jet. Additionally, an arrangement was tried (Fig. 6c) where the spray gas was flushed through the shroud to provide inert gas for the turbulent mixing of the jet. In this arrangement, the shroud is attached to the nozzle and moves with it. Although the distance between nozzle and substrate is kept as constant as possible in the robotic operation, a gap always remains between shroud and substrate. Thus, it is practically impossible to prevent contact between the surrounding atmosphere and the jet or the hot deposit, but the shroud protects the jet rather well when and after it leaves the nozzle (and is still slow, hot, and reactive). Turbulence might draw in some of the surrounding atmosphere near the substrate, but there the temperature of the droplets and thus the rate of oxidation are already lower. More importantly, the atomization and shroud gas flow rates are large enough to force a net outflow of gas from the shroud/substrate gap. Further, observation shows that particles emerging from the shroud/substrate gap are essentially all overspray; none adheres to the substrate or is otherwise incorporated in the shell.

In these three arrangements three different gases were used: air, nitrogen, and argon. The change from the air to nitrogen cuts down the oxygen partial pressure by a factor of five at reasonable cost, whereas the change from nitrogen to the heavier argon increases cost dramatically but further reduces the oxygen exposure. In addition, the use of argon prevents potential problems with nitride formation in the ferrous systems (Ref 21), and the arc is much more stable in an argon atmosphere than in a nitrogen atmosphere (Ref 22).

The metal deposition schedule for these experiments was:

- Step 1: Arc spray a path consisting of 12 cycles of back-and-forth motion across a substrate (7 mm low-carbon steel plate in most cases).
- Step 2: Wait for the temperature of the sprayed shell to return from its heated state (typically 60 °C) to some nominal level (typically 40 °C).
- Step 3: Repeat until adequate shell thickness for sectioning was reached. Generally, this procedure was repeated eight to ten times, producing a typical shell thickness of 1.3 mm.

Various materials were sprayed (compositions are in weight percent):

- Plain carbon steel 1080 (0.8 % C, remainder iron)
- Martensitic type 420 stainless steel (0.15% C min, 1% Mn, 1% Si, 12 to 14% Cr, 0.04% P, and 0.03% S)
- Bronze (2% Si, remainder copper)
- Invar (36% Ni, remainder iron)

These materials were sprayed onto mild steel that had been glass-bead peened.

The samples sprayed in a completely inert atmosphere were formed in a closed vacuum chamber. The chamber was evacuated to 0.7 kPa (5 torr), then backfilled to 57 kPa (430 torr) with argon. The arc-spray gun was inserted into the chamber, and during spraying a vane vacuum pump was used to hold the pressure at 57 kPa. The atomization gas for these experiments was argon, and the wire guide tubes were pressurized by argon as well. The substrate for these experiments was a 46 cm diam mandrel.

4. Characterization of Spray

4.1 *Particle Velocity*

Spray from the arc-spray gun is shown in Fig. 7. This photograph was taken with the focal-plane shutter moving perpendicularly to the direction of travel of the sprayed particles; the exposure time was 250 μs. The photo shows the irregular nature of the arc spray; the process sputters along, rather than continuously depositing a fine shower of metal. A gap in the stream of spray is noticeable 25 cm from the arc. It is also apparent that particles along the periphery of the spray cone are moving more slowly than those along its axis.

Particle velocity, as inferred from the length of particle streaks (Fig. 7), is measured between 40 and 70 m/s. This speed, of course, varies as the particles leave the arc near zero velocity

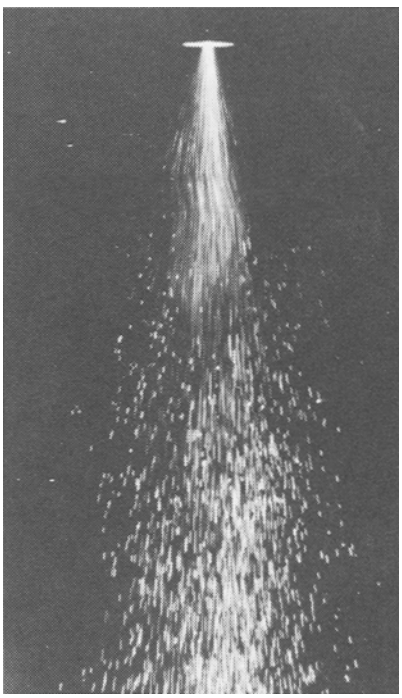

Fig. 7 Spray of type 420 stainless steel in air with air atomization

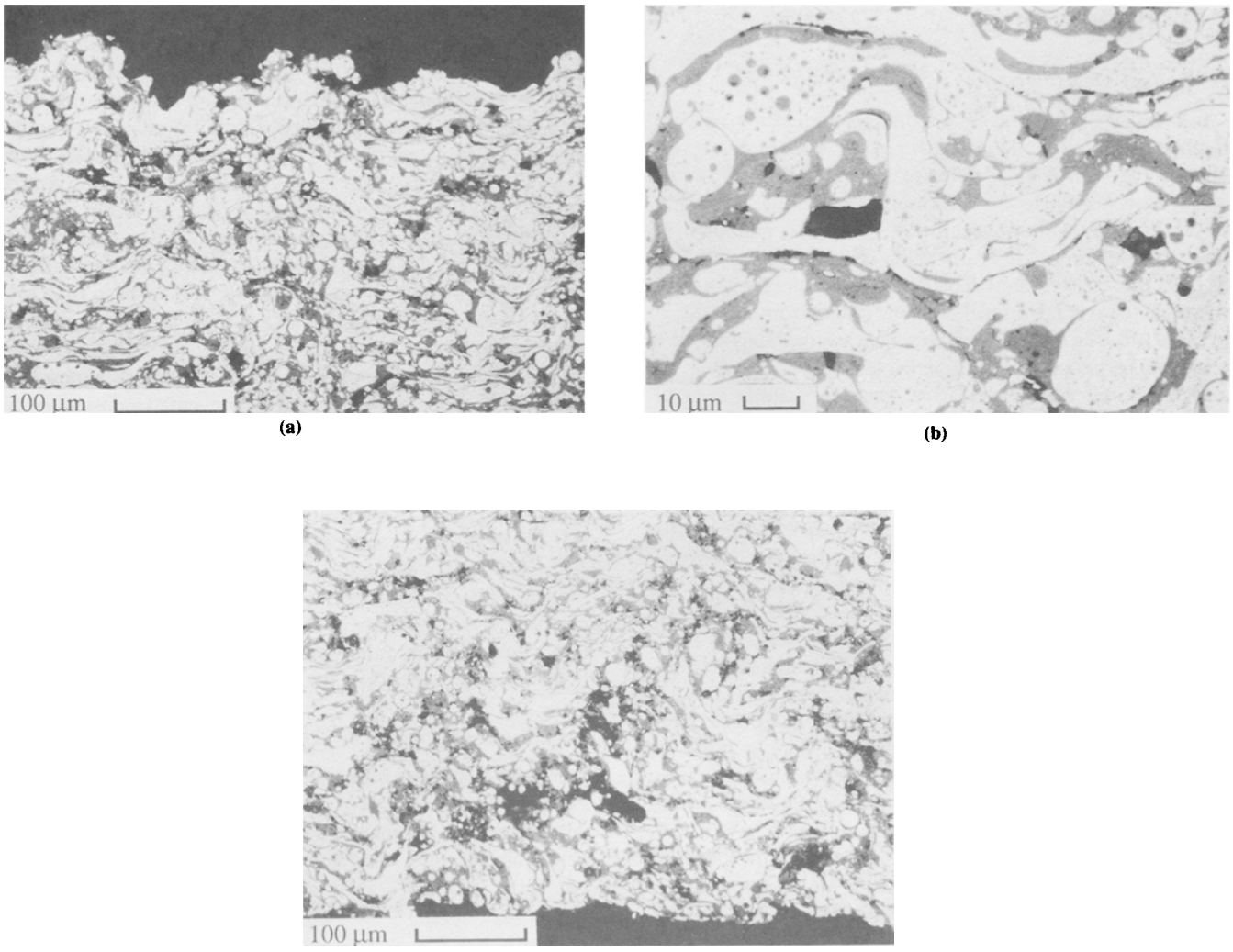

Fig. 8 Optical micrographs of the cross section of 6 mm of deposited Invar. (a) Last deposited material near shell surface. 200×. (b) Center of deposited material. 1000×. (c) First deposited material near substrate interface

of course, varies as the particles leave the arc near zero velocity (at the wire-feed speed), accelerate in the gas stream moving at subsonic velocity, and then, as the gas stream disperses and slows, decelerate from the resistance of the gas stream. The speed of the particles should also be strongly influenced by their particular size, which, in turn, is influenced by the atomization gas pressure. Mathur et al. (Ref 9) discuss atomized particles in a gas stream in some detail in reference to the Osprey process. As far as aerodynamics is concerned, there is little difference between the arc-spray process and the Osprey process. The velocity measurements from Fig. 7 and the micrographs in section 5 of this paper show the same regime as the Osprey process: 10 to 20 μm diam droplets move at a speed of 40 to 70 m/s. However, particle flux is lower and particle temperature is higher.

4.2 *Material Buildup*

The arc-spray system builds up shells by depositing particles onto the substrate. They individually splat quench; there is never a complete liquid layer on the surface of the deposit in this process at the material deposition rates under consideration. The deposit is created by the buildup of these individually solidified particles. Arata et al. (Ref 23) report that particles in the arc-spray system cool within 125 μs of impact on a substrate. This suggests that these particles are cooling at a rate of at least 10^4 K/s. The resulting solidification rates are 25 cm/s. Moreau et al. (Ref 24) have shown cooling rates in individual lamellae of molybdenum and partially stabilized zirconia at 10^8 K/s, measuring the temperature evolution and showing that solidification is complete in 20 μs. This suggests solidification rates of about 150 cm/s. The substrate receiving the arc-sprayed droplets is as cold as a substrate in splat-quench ribbon-producing systems, but the droplets in the arc-spray configuration are much smaller. Therefore, cooling rates of at least 10^4 to 10^6 K/s can be achieved. These high cooling rates allow, in principle, deposition of metastable or quasi-crystalline alloys with interesting properties (Ref 25, 26).

5. Microstructure

5.1 *Optical Metallography*

In order to discuss the essential features observed, the micrograph of the Invar alloy is shown in Fig. 8 (at high magnification in Fig. 8b). The deposit is reasonably uniform from the first layers deposited to the last deposited, as shown in Fig. 8(a) and (c). Figure 8(b) shows that the total deposit is built up of lamella that range from 4 to 10 μm in thickness and from 50 to 100 μm in length. Each of these lamella is a solidified droplet, indicating that the average droplet diameter ranges from 10 to 20 μm up to 100 μm. The largest lamella in these micrographs suggests an original particle diameter of perhaps 140 μm.

Figure 8 indicates several facts. Droplets solidify in isolation; there has never been a liquid pool on the surface. The uniformity of the size distribution implies that splashing is not important: Upon impinging on the surface, droplets do not fragment but flatten out to lamellae before they solidify. The arc-spray gun was oriented so that the particles arrived normal to the surface for the material sprayed in this sample. Three different shades of gray are visible in Fig. 8, particularly Fig. 8(b): white, gray, and black. By x-ray energy-dispersive analysis (Fig. 9), the white area was verified as being metal, the gray areas as oxide, and the black areas as pores. The original composition of Invar is Fe-36 wt% Ni; the composition has been changed in this sample by the heavy oxidation (roughly 30% oxide). The bright regions are about Fe-40 wt% Ni, and the dark regions are roughly Fe-18 wt% Ni. Nickel oxidizes more slowly than iron, so it is not surprising that the oxide regions are predominantly iron. If, however, the goal of spraying Invar was to have a shell made of a material with a low coefficient of thermal expansion, then this goal cannot be met by spraying in air; the composition change has moved the alloy away from the Invar effect.

The morphology of the oxide particles raises an interesting question. How was the formation of lamellae (and not spheres) of oxide possible? If liquid-metal droplets had hit the surface and had splat out into lamellae before becoming oxidized, one would expect the lamellae to be surrounded by oxide, producing a microstructure with intergranular oxide and, presumably, undesirable mechanical properties. The presence of oxide lamellae indicates another mechanism: Metal droplets have oxidized in the arc and in flight between the nozzle and the substrate, forming droplets of liquid oxide that hit the surface and squash out to lamellae. The discussion in section 4.1 indicates that the droplets spend about 3 ms in flight; they have been heated to less than the arc temperature of 10^4 K (Ref 14), but more than the oxide liquidus (1670 K for Fe_3O_4, and 1830 K for FeO). Apparently these liquid iron droplets can oxidize to liquid Fe_3O_4, Fe_2O_3, and FeO while being kept well superheated for 3 ms.

5.2 *Oxide*

The oxide and porosity levels (expressed as a percent area of the field of view) in the deposited shells are shown in Fig. 10 along with micrographs of these shells. The oxide and porosity measurements shown were performed using an image analysis program analyzing scanned images from photomicrographs. The level of uncertainty in these measurements is high. Fowler et al. (Ref 27) have shown that with eight repetitions on a single sample, it is possible to operate within a 95% confidence band for porosity measurements, but oxide measurements require more repetitions. This can be seen in the data in the 0.8% C steel column; the oxide and porosity values vary in unexpected ways compared to the other materials. Furthermore, spray-gun designs greatly influence the porosity and oxide levels in the sprayed shell. The measurements here, therefore, should only be used to represent the trends that are possible with inert gases.

With the open, unprotected arrangement of Fig. 6(a) an oxide content of approximately 30% is obtained for both steels and the Invar alloy if air is used for atomization. This drops to 10 to 15% oxide for a nitrogen atomization gas in an air environment. If oxidation had occurred only in the nozzle, no oxidation should have occurred at all, but the turbulence of the air atmosphere still causes oxidation. This is largely prevented by using the arrangement shown in Fig. 6(b), or the better arrangement depicted in Fig. 6(c). These decrease the oxidation content to about 8%. If argon is used in the nozzle with the protective scheme shown in Fig. 6(b) or (c), the oxide content falls to less than 8%. If the experiment is conducted in a vacuum chamber backfilled with argon, the oxide content drops to less than 2%, but this arrangement is experimentally expensive. In the argon-backfilled chamber, the measurement of oxide reflects wire contamination, or microporosity that appears to be oxide at optical magnification levels, rather than in-spray-formed oxide.

5.3 *Metallography by Scanning Electron Microscopy*

Figure 11 shows a backscatter image of the sprayed eutectoid steel (0.8% C). Depending on the quench rate and the temperature history of the material, several phases and mixtures of phases are possible: pearlite, a mixture of ferrite (α) and cemen-

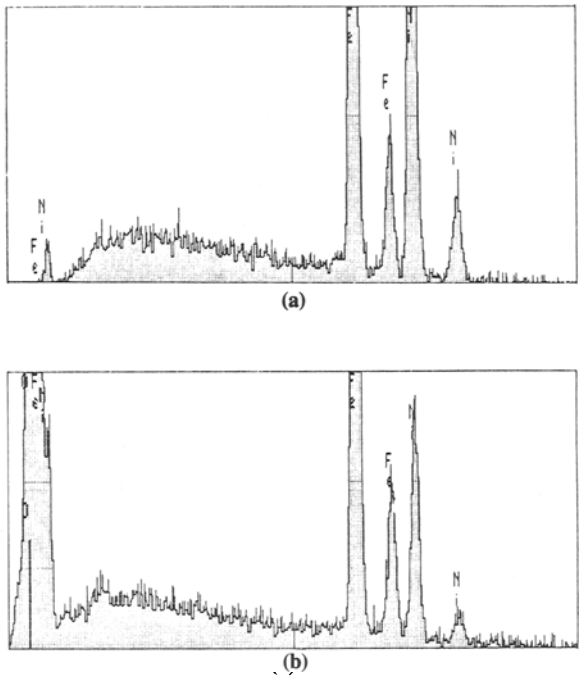

Fig. 9 X-ray energy-dispersive analysis of atmosphere-sprayed Invar. (a) Spectrum for bright (metal) regions. (b) Spectrum for dark (oxide) regions

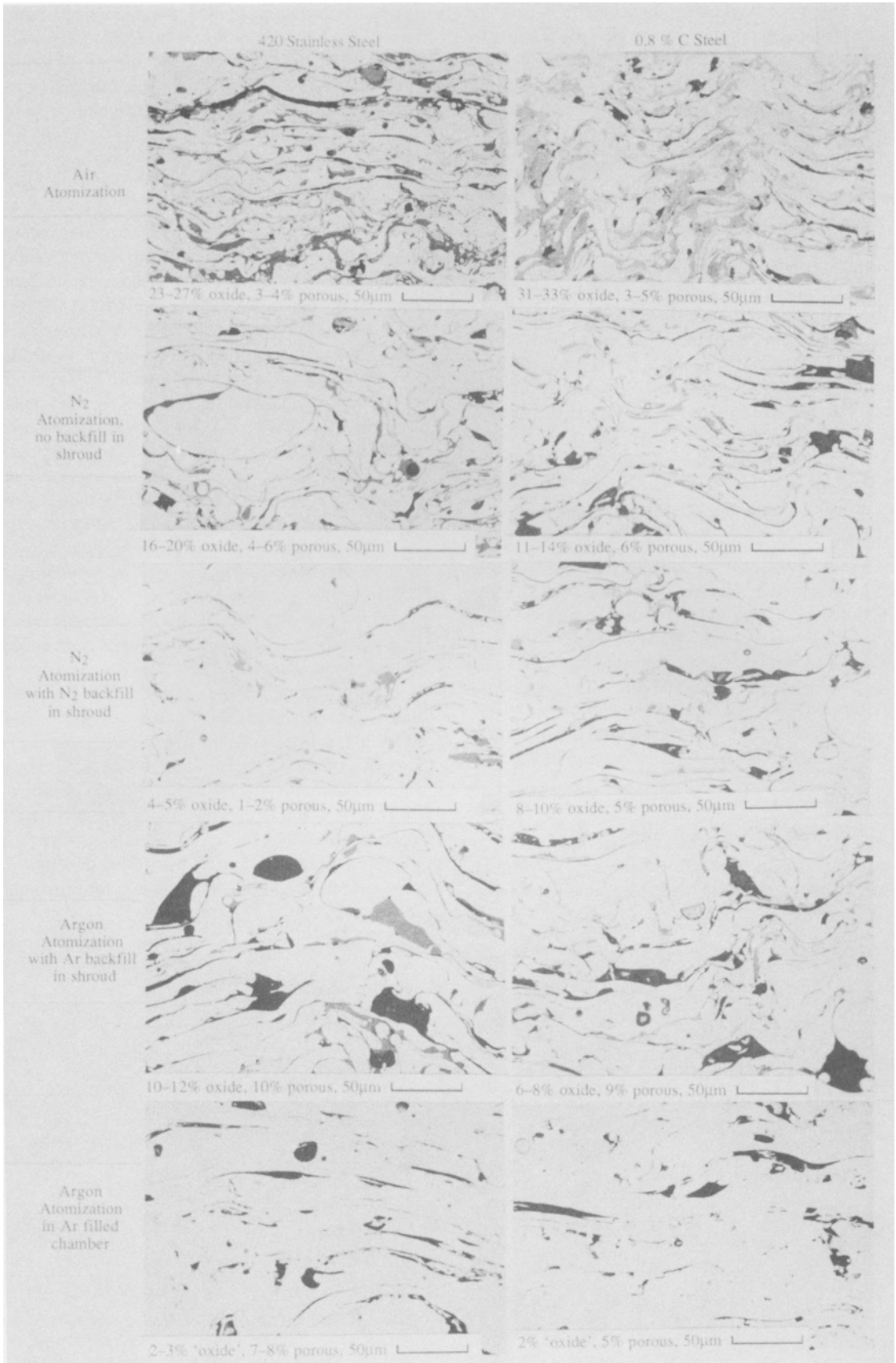

Fig. 10(a) Metallographic sections of the 0.8% C steel and type 420 stainless steel deposits

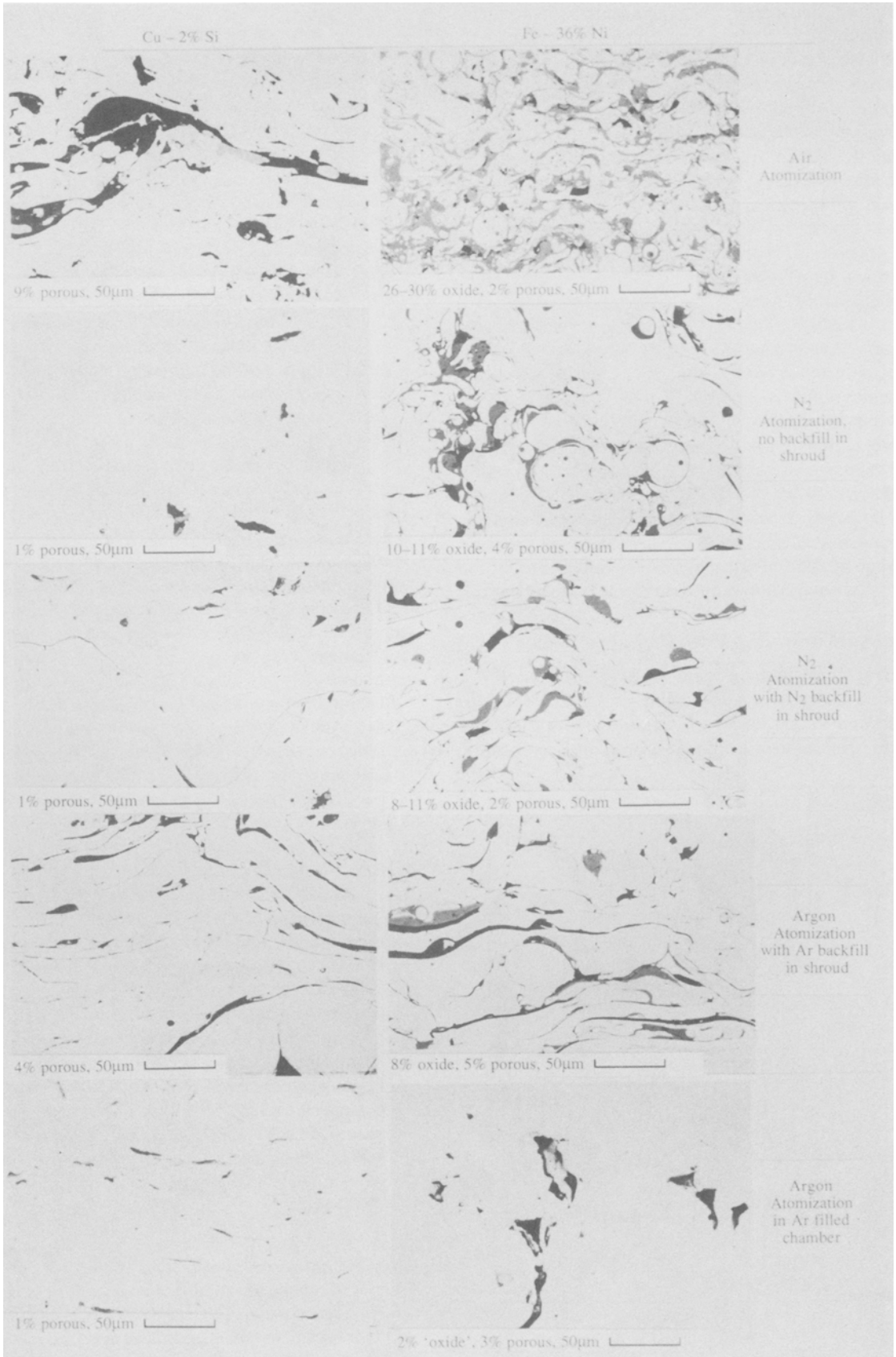

Fig. 10(b) Metallographic sections of the copper and Invar deposits

tite (Fe_3C), upper bainite, lower bainite, martensite, and retained austenite (γ) (Ref 28). For this composition of steel, pearlite and the bainite transformations can be avoided if the cooling rate from 996 to 473 K is at least 200 K/s (Ref 29). If the cooling rate is much faster, martensite particle formation will be suppressed as well (Ref 30, 31). The 25 μm particle in the center of Fig. 11 shows an already solidified particle when it arrived at the substrate. This particle is composed entirely of retained austenite. The lamella below and surrounding the particle arrived at the substrate in a molten state, and subsequently solidified. The cooling of this lamella was such that martensite particles formed in the last deposited (upper) portion of the lamella, while the lower region of the lamella consists of retained austenite. This indicates that the cooling rate was highest near the lamella/substrate interface and that the region of the splat away from the interface remained longest at high temperature. The lamellae and particles in Fig. 11 probably arrived at the substrate nearly simultaneously; the solidified particle forced itself onto the previously arrived lamella, forcing the liquid surface up and around. In the larger lamella of Fig. 11, small pores, on the order of 0.1 to 0.5 μm in diameter, are also visible. These appear in all of the sprayed materials from this process, and are an artifact of the violence of the ablation and atomizing processes.

The microstructure in the lamellae of arc-sprayed material is similar to the structure of splat-ribbon materials, with the distinction that the interfaces between the lamellae are much worse. The production of splat ribbons is a continuous-casting process. The arc-spray process deposits liquid droplets individually on the solid surface; each of these droplets undergoes thermal stresses during cooling, and this can lead to decohesion or microcracking along the lamella/lamella interface. The usual consolidation methods, such as hot isostatic pressing or forging (cold or hot working), are in conflict with the intentions for this sprayed material, and thus more subtle methods such as laser glazing or shot peening of each layer could and should be used. For the unconsolidated deposits shown or discussed in this paper, the mechanical properties are controlled not by the behavior of the individual lamellae, but by the strength of the interfaces between them. The presence of interlamella microcracks might be detrimental in tension, but is of no concern for metal shells subjected to compression.

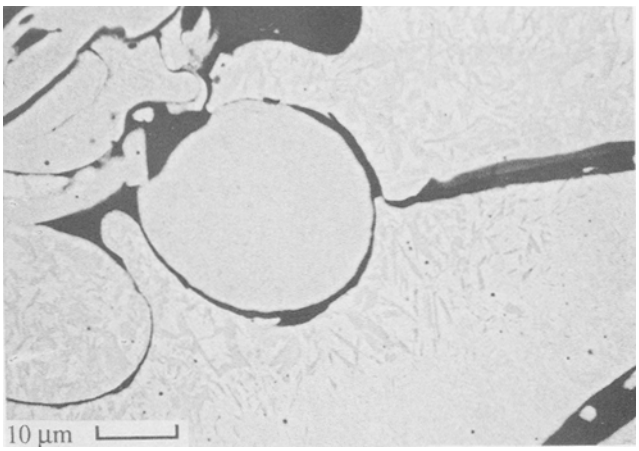

Fig. 11 Scanning electron micrograph of the sprayed 0.8% C steel showing martensite formation surrounded by retained austenite. The martensite particles are acicular in appearance in this section (probably being lenticular in three dimensions) and vary in size. They are on the order of 0.5 by 4 μm.

6. Composite Structures

Given the layered and disjointed lamellae formed in the arc-spray process, even when sprayed in oxygen-free environments, processes to control the microstructure without cold or hot working the entire shell must be developed. As discussed in section 2.2.1 and given in Table 1, a number of process parameters can be manipulated to affect the particles forming the lamella. Beyond the arc-spray process parameters, there are two compatible directions to follow: control the material properties by altering the materials deposited, and control the position and orientation of the lamella to improve the shell characteristics. The goal is to tune the material in the shell so it more successfully meets the demands of the application.

6.1 *Sprayed Composite Materials*

One microstructure experiment has been to create a stratified shell, with each stratum being made of a distinct material. Figure 12 shows a structure made of alternating layers of 0.8% C steel and Invar. The sample has been etched with picral for 15 s to darken the steel. Each layer is about 0.15 mm (0.006 inch) thick.This sample was sprayed using argon atomization gas, a shroud, and an argon-backfilled shroud. Figure 13 shows a detail of the mixing region of the two materials. There are no difficulties in the interlayer bonding of this material, even though perhaps 15 min passed between the deposition of the layers.

6.2 *Pseudoalloy*

In another microstructure experiment, a shell of blended materials was created. The arc-spray process forms an arc between two feed wires to melt them; it is possible to use two wires of dif-

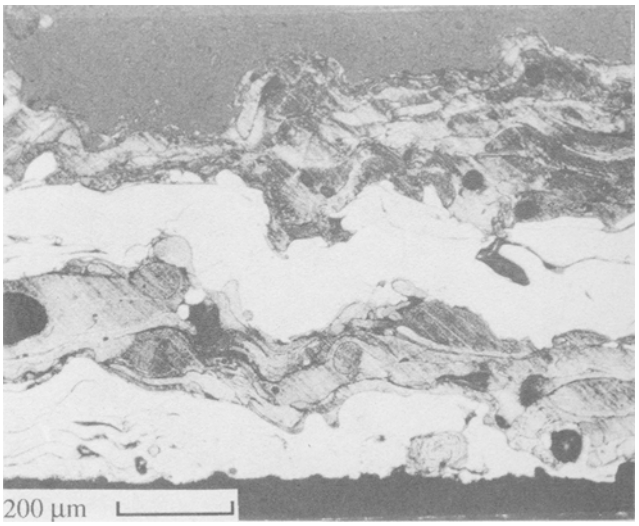

Fig. 12 Composite layered structure of 0.8% C steel and Invar

ferent material. Figure 14 shows a shell made by mixing 0.8% C steel and Invar. The sample in Fig. 14 was sprayed using argon atomization gas, a shroud, and an argon-backfilled shroud.

The nature of this mix is entirely different from that of the layered composite. The particles arriving molten still form flat lamellae in the deposit, but the distinct layering of lamellae is replaced by a random mixture of lamellae. In Fig. 14, the particles are arriving nearly simultaneously, and the bonding of the lamellae is similar to that of the layered composite, as seen in Fig. 15.

From Fig. 14, it is evident that the lamellae are either Invar or iron. Apparently droplets detach themselves individually either from the steel or the Invar wire feeding the arc, and there is little opportunity for the individual particles to mix either in flight or on the substrate; the solidification rates are sufficient on the substrate to prevent mixing there. X-ray mapping of this deposit has verified that little mixing of the Invar and iron has occurred.

6.3 *Oriented Lamellae*

A shell composed entirely of lamellae oriented in one direction may show good resistance to stresses in that direction, but will also be weak to stresses applied in other directions. Appropriate control of the orientation of the lamellae in a layer will improve shell characteristics; this is especially interesting when the orientations and positions of the lamellae are designed for specific structural features.

6.3.1 Stratified Orientations

The experiment shown in Fig. 16 demonstrates a series of stratum, each with a new lamella orientation. The robot was used to systematically apply the material; the lamellae are rotated about ±25° from the horizontal. Figure 17 shows a detail of the mixing between the strata. There is mixing of lamellae in

Fig. 13 Detail of interface between 0.8% C steel and Invar in layered composite

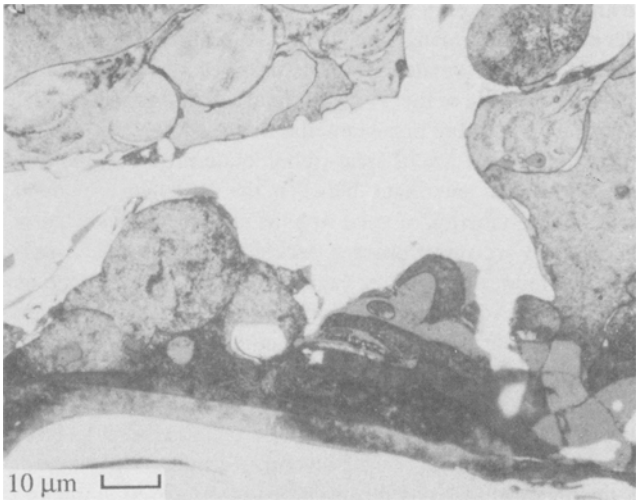

Fig. 15 Detail of interlamella region in pseudoalloy of 0.8% C steel and Invar

Fig. 14 Mixed pseudoalloy of 0.8% C steel and Invar

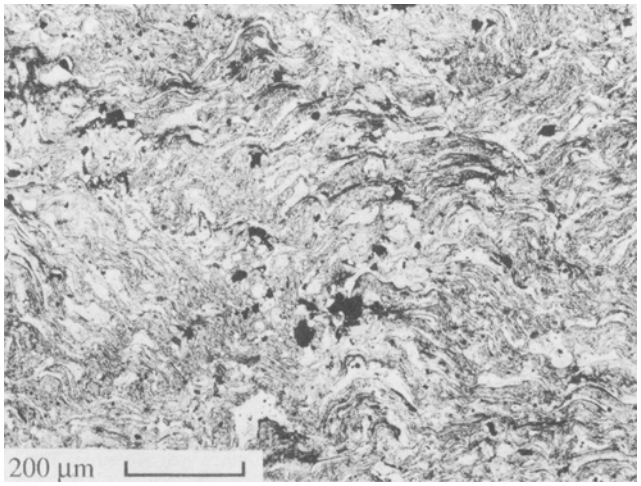

Fig. 16 Oriented lamellae of 0.8% C steel

this region, so there should be good vertical bonding of the strata in the composite structure.

An effort was made in spraying the shell shown in Fig. 18 to remove some of the porosity by mechanically shot peening each layer after it was sprayed. Shot peening also changes the state of stress in the shell, but this is not visible in optical metallography. In samples that are made by metal atomized by air, shot peening also removes some of the oxide on the surface.

The samples in these figures were sprayed with air atomization and no shroud. Comparison of Fig. 16 and 18 shows that peening the surface between each oriented layer causes the following reductions: from an initial 13 to 15% porosity to a final 7 to 9% porosity, and from an initial 34 to 36% oxide to a final 30 to 32% oxide.

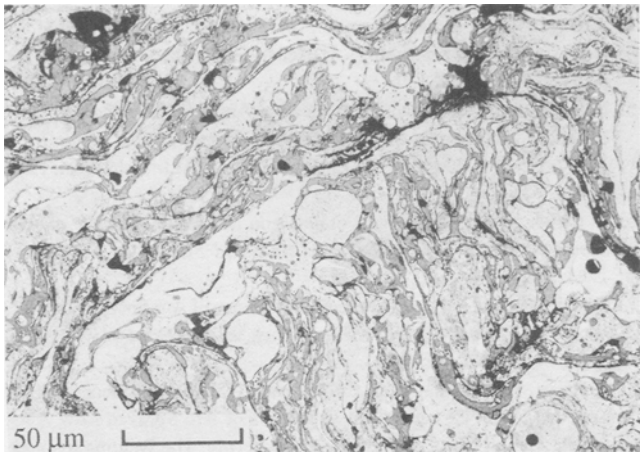

Fig. 17 Detail of Fig. 16 showing oriented lamellae of 0.8% C steel

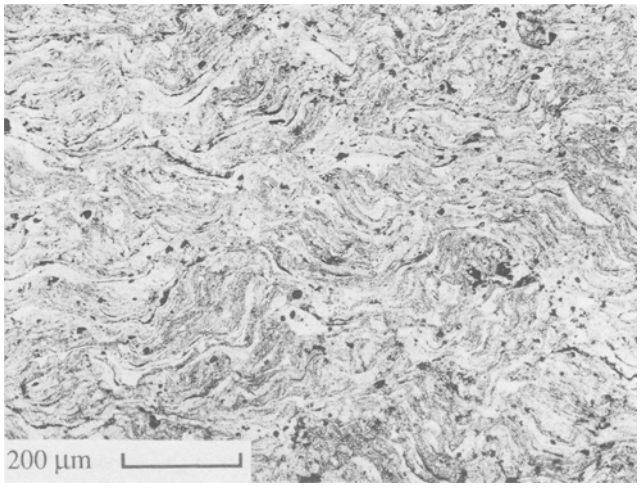

Fig. 18 Oriented lamellae of 0.8% C steel with glass peening between each layer

6.3.2 Flow of Lamella around Features

The shells created by metal spraying normally include stress-concentrating geometries—in particular, sharp corners. Arbitrary spraying onto these stress-concentrating features of the substrate can create microstructures similar to that shown in Fig. 19. This structure will not withstand corner loading with any measure of success. As a matter of fact, the material in Fig. 19 cracked during preparation. Figure 20 shows the same geometry, but a different spray strategy; the lamellae were oriented to flow over the corner and thus present some structure to withstand the loading in the corner. Judicious control of the microstructure around asperities, wedges, corners, and similar features is essential for ensuring good mechanical behavior of the shell. The necessary intricate movements of the nozzle over

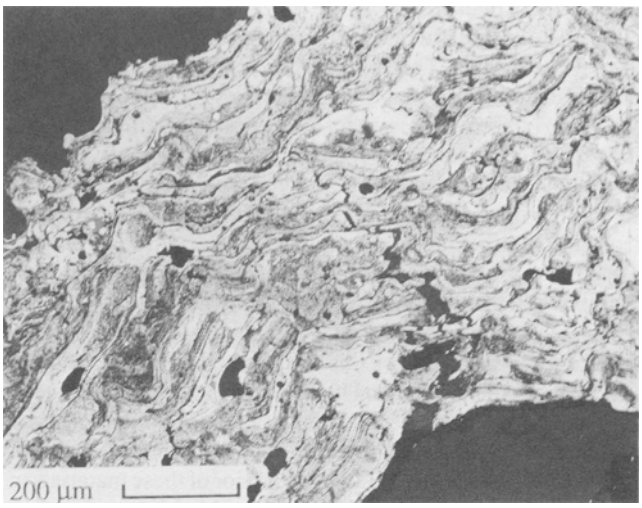

Fig. 19 Lamellae sprayed around a corner

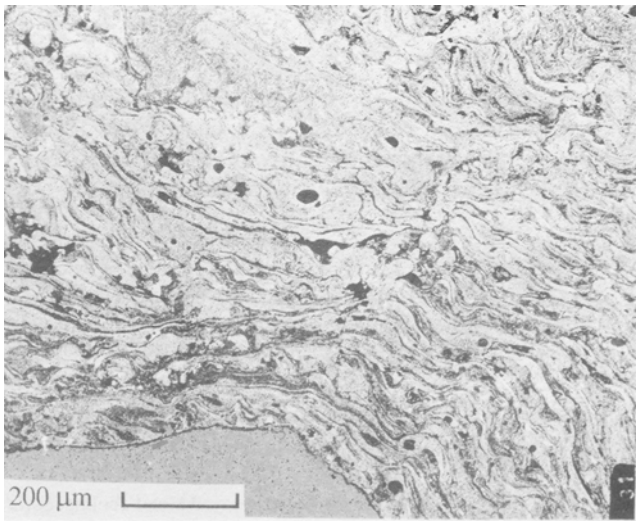

Fig. 20 Flow of oriented lamellae around a corner

the geometric features of the shell are accomplished most effectively by a robotic manipulator.

7. Conclusion

The arc-spray process results in a "quilt" of quickly solidified lamellae laced together into a relatively weak structure—a sort of three-dimensional jigsaw puzzle. Traditionally, this type of quilt is soaked and then hot and cold worked to dissolve impurities; all memory of the porosity and grain-boundary imperfections is erased in such processes.

The authors are applying the arc-spray process to quickly and repeatably create precise shapes; the specific goal is to make tooling shapes for molds. Soaking and working are in conflict with the goals of speed and precision; fortunately, the demands of tooling are centered around hoop stresses, compressive loading, and wear. The sprayed metals produce shells that lend themselves to these demands.

To create successful materials in a sprayed shell, the levels of oxide are controlled. That is, some oxide is permitted to remain; these oxides are hard, wear resistant, and fully supported by the metal matrix surrounding them. The microstructure is further tailored to meet geometry requirements in the shell. Finally, these shells can be composed of composite structures, both in the sense of a variety of materials either mixed together or placed in stratified layers, and in the sense of differing lamella orientations. This oriented structure is created most consistently by robotically manipulating the spray device.

This work is part of a more comprehensive research effort. The next steps, as guided by this microstructural understanding, must focus on the mechanical behavior of these sprayed materials, paying particular attention to the loading modes and wear conditions that are present in tooling applications. Future work will also concentrate on the failure behavior of these materials in the shells under service conditions; from this information, further design of the material will improve the robustness of the tooling. The result will be insight into the design and fabrication of microstructure and mechanical behavior to give a firm foundation upon which to rapidly build useful sprayed metal shells.

Acknowledgments

This work has been supported by the Aluminum Company of America, by Carnegie Mellon University under a DARPA contract for Shaping by Deposition, and by the Engineering Design Research Center, an NSF Engineering Research Center.

References

1. L.E. Weiss, E.L. Gursoz, F.B. Prinz, P.S. Fussell, S. Mahalingam, and E.P. Patrick, A Rapid Tool Manufacturing System Based on Stereolithography and Thermal Spraying, *Manuf. Rev.*, Vol 3(No. 1), 1990, p 40-48
2. *Metallizing Manual*, Metallizing Company of America, 1963
3. T.H. Turner and N.F. Budgen, *Metal Spraying*, Charles Griffin & Co., London, 1926
4. P.S. Fussell and L.E. Weiss, Steel-Based Sprayed Metal Tooling, *Solid Freeform Fabrication Symposium*, J.J. Beaman, H.L. Marcus, D.L. Bourell, and J.W. Barlow, Ed., University of Texas—Austin, 1990, p 107-113
5. P.S. Fussell, et al., A Sprayed Steel Tool for Permanent Mold Casting of Aluminum, *1991 SAE Aerospace Atlantic*, SAE International, 1991
6. E.L. Gursoz, Y. Choi, and F.B. Prinz, Vertex-based Representation of Non-manifold Boundaries, *Geometric Modeling for Product Engineering*, M.J. Wozny, J.U. Turner, and K. Preiss, Ed., Elsevier Science, 1990
7. S.C. Gill and T.W. Clyne, Stress Distributions and Material Response in Thermal Spraying of Metallic and Ceramic Deposits, *Metall. Trans. B*, Vol 21B, 1990, p 377-385
8. E.J. Lavernia and N.J. Grant, Spray Deposition of Metals: A Review, *Mater. Sci. Eng.*, Vol 98, 1988, p 381-394
9. P. Mathur, D. Apelian, and A. Lawley, Analysis of the Spray Deposition Process, *Acta Metall.*, Vol 37(No. 2), 1989, p 429-443
10. D. Apelian, M. Paliwal, R.W. Smith, and W.F. Schilling, Melting and Solidification in Plasma Spray Deposition—Phenomenological Review, *Int. Met. Rev.*, Vol 28(No. 5), 1983, p 271-293
11. P. Fauchais, A. Grimaud, A. Vardelle, and M. Vardelle, Plasma Spraying: An Overview, *Ann. Phys. (Paris)*, Vol 14(No. 3), 1989, p 261-310
12. H. Herman, Plasma Sprayed Coatings, *Sci. Am.*, Vol 256 (No. 9) 1988, p 112-117
13. E. Pfender, Fundamental Studies Associated with the Plasma Spray Process, *Surf. Coat. Technol.*, Vol 34(No. 1), 1988, p 1-14
14. S. Safai and H. Herman, Plasma-Sprayed Materials, *Treatise on Materials Science and Technology*, H. Herman, Ed., Academic Press, 1981, p 183-214
15. M.L. Thorpe, How Recent Advances in Arc Spray Technology Have Broadened the Ranges of Applications, *Thermal Spray Technology: New Ideas and Processes*, D.L. Houck, Ed., ASM International, 1989, p 375-383
16. L. Cifuentes and S. Harris, Composition and Microstructure of Arc-Sprayed 13% Cr Steel Coatings, *Thin Solid Films*, Vol 118(No. 4), 1984, p 515-526
17. S. Harris and M.P. Overs, Oxidation Behavior of Arc Sprayed Iron and Nickel Alloy Coatings, *Thin Solid Films*, Vol 118(No. 4), 1984, p 495-505
18. S. Harris, L. Cifuentes, R.C. Cobb, and D.H. James, Influence of Heat Transfer on the Structure and Properties of Arc Sprayed Low Alloy Steels, *1st Int. Conf. on Surface Engineering*, The Welding Institute, Brighton, UK, 1985, p 79-94
19. S.J. Harris, L. Cifuentes, and D.H. James, The Use of a Computer Model of the Metal Arc Spray Process to Produce Improved Coating Properties, *Advances in Thermal Spraying*, Pergamon Press, Oxford, 1986
20. J.J. Kaiser and R.A. Miller, Inert Gas Improves Arc-Sprayed Coatings, *Adv. Mater. Process.*, Vol 136(No. 6), 1989, p 37-40
21. W. Milewski and M. Sartowski, Some Properties of Coatings Arc-Sprayed in Nitrogen or Argon Atmosphere, *Advances in Thermal Spraying*, Pergamon Press, Oxford, 1986, p 467-473
22. R. Kawase and K. Maehara, Arc Spraying Method Using Argon as Atomizing Gas, *J. High Temp. Soc. Jpn.*, Vol 10(No. 6), 1984, p 284-290
23. Y. Arata, A. Ohmori, J. Morimoto, A. Yamaguchi, and R. Kawase, Dynamic Behavior of High Energy Thermal Spraying, *Advances in Thermal Spraying*, Pergamon Press, Oxford, 1986, p 485-493
24. C. Moreau, M. Lamoutagne, and P. Cielo, Influence of the Coating Thickness on the Cooling Rates of Plasma-Sprayed Particles Impinging on a Substrate, *Thermal Spray Research and Applications*, T.F. Bernecki, Ed., ASM International, 1991, p 237-244
25. K.H. Kuo, Quasicrystals, *International Workshop on Quasicrystals*, Trans Tech Publications, Beijing, 1987, p 651
26. P.J. Steinhardt and S. Ostlund, *The Physics of Quasicrystals*, World Scientific Publishers, 1987
27. D.B. Fowler, W. Riggs, and J.C. Russ, Inspecting Thermally Sprayed Coatings, *Adv. Mater. Process.*, Vol 141(No. 11), 1990, p 41-52

28. W. Hume-Rothery, in *The Structures of Alloys of Iron*, Pergamon Press, Oxford, 1966, p 221
29. M.F. Ashby and D.R.H. Jones, in *Engineering Materials 2*, Pergamon Press, Oxford, 1986, p 78
30. B. Cantor, Rapid Solidification of Steels, *Rapidly Solidified Amorphous and Crystalline Alloys*, B.H. Kear, B.C. Giessen, and M. Cohen, Ed., Elsevier Science, 1982, p 317-330
31. K. Murakami, H. Asako, T. Okamoto, and Y. Miyamoto, Microstructure and Mechanical Properties of Rapidly Solidified Deposited Layers of Fe-C-Cr Alloys Produced by Low Pressure Plasma Spraying, *Mater. Sci. Eng. A*, Vol 123, 1990, p 261-270